JOURNAL OF SPACECRAFT AND ROCKETS
Vol. 44, No. 1, January–February 2007

Formation and Attitude Control for Rotational Tethered Satellite Clusters

Osamu Mori*
Japan Aerospace Exploration Agency, Kanagawa 229-8510, Japan
and
Saburo Matunaga†
Tokyo Institute of Technology, Tokyo 152-8552, Japan

A tethered satellite cluster system, which consists of a cluster of satellites connected by tethers and which can maintain and change formation via active control of tether tension and length to save thruster fuel and improve control accuracy is proposed. The concept can be applied to tethered multisatellites for in-orbit servicing, which can perform various missions, including inspection, casting, capture, recovery, moorage, and deorbiting of an uncontrolled satellite. The rotational motion of such a system that the satellites in formation flying are required to rotate about the center of mass of the system on the same desired plane is considered. The equilibrium conditions that the tether tension imposes on the rotational motion are given, and a coordinated control method for the thrusters, the reaction wheels, and the tether tension/torque is proposed. Numerical simulations and ground experiments show that the control of the tether tension and torque not only saves thruster fuel, but also improves the position and attitude accuracy of formation flying.

Nomenclature

$\boldsymbol{a}_{jk} = \{\boldsymbol{i}\}^{T_i} a_{jk} = \{\boldsymbol{b}_j\}^{T_b} a_{jk}$	=	vector from the c.m. of satellite j to the end of arm jk
$\{\boldsymbol{b}_j\} = \{\boldsymbol{b}_{j_x}\ \ \boldsymbol{b}_{j_y}\ \ \boldsymbol{b}_{j_z}\}^T$	=	body-fixed coordinate system of satellite j
C, K	=	derivative/proportional gains
$C^j(\theta)$	=	coordinate transformation matrix around the axis j of angle θ
d_j	=	distance from the origin of $\{\boldsymbol{r}\}$ to the c.m. of satellite j in plane
$\boldsymbol{F}_j = \{\boldsymbol{i}\}^{T_i} F_j$	=	force vector acting on satellite j as the result of the thruster
$\boldsymbol{F}_{jk}, \boldsymbol{\tau}_{jk}$	=	force/torque vectors on satellite j caused by the tension of tether jk
H_j	=	foot of perpendicular from the c.m. of satellite j to the rotational plane
h_j	=	height of the c.m. of satellite out of plane
$\boldsymbol{I}_j = \{\boldsymbol{b}_j\}^{T_b} I_j \{\boldsymbol{b}_j\}$	=	moment of inertia about a set of axes passing through the c.m. of satellite j
$\{\boldsymbol{i}\} = \{\boldsymbol{i}_x\ \ \boldsymbol{i}_y\ \ \boldsymbol{i}_z\}^T$	=	Earth-centered inertial coordinate system
l_{jk}	=	distance between the c.m. of satellite j and the end of arm jk
m_j	=	mass of satellite j
$\boldsymbol{P}$	=	angular momentum vector about the c.m. of tethered satellite cluster system
$\boldsymbol{q}_{\text{c.m.}} = \{\boldsymbol{i}\}^{T_i} q_{\text{c.m.}}$	=	c.m. of tethered satellite cluster system
$\boldsymbol{q}_j = \{\boldsymbol{i}\}^{T_i} q_j = \{\boldsymbol{b}_j\}^{T_b} q_j$	=	position vector of the c.m. of satellite j
$\{\boldsymbol{r}\} = \{\boldsymbol{r}_x\ \ \boldsymbol{r}_y\ \ \boldsymbol{r}_z\}^T$	=	rotational coordinate system
$\{\boldsymbol{s}\} = \{\boldsymbol{s}_x\ \ \boldsymbol{s}_y\ \ \boldsymbol{s}_z\}^T$	=	intermediate coordinate system fixed on the desired rotational plane
T_{jk}	=	tension of tether jk
α_j, β_j	=	length of the major/minor axis of the ellipse of satellite j
λ_j	=	angle between the two directions of satellites j and 1 in plane
$\boldsymbol{\tau}_j = \{\boldsymbol{b}_j\}^{T_b} \tau_j$	=	torque vector acting on satellite j as the result of the reaction wheel
$\varphi_r, \theta_r, \psi_r$	=	3-2-1 Euler angles between $\{\boldsymbol{r}\}$ and $\{\boldsymbol{i}\}$
$\dot{\varphi}_r$	=	spin angular velocity of $\{\boldsymbol{r}\}$ with respect to $\{\boldsymbol{s}\}$
$\psi_j, \theta_j, \varphi_j$	=	1-2-3 Euler angles between $\{\boldsymbol{b}_j\}$ and $\{\boldsymbol{r}\}$
$\boldsymbol{\omega}_j = \{\boldsymbol{b}_j\}^{T_b} \omega_j$	=	angular velocity vector of satellite j

Presented as Paper 2001-4392 at the AIAA Guidance, Navigation, and Control Conference, Montreal, Quebec, Canada, 6–9 August 2001; received 4 December 2004; revision received 28 June 2005; accepted for publication 21 July 2005.

*Research Associate, Institute of Space and Astronautical Science, 3-1-1 Yoshinodai, Sagamihara. Member AIAA.

†Associate Professor, Department of Mechanical and Aerospace Engineering, 2-12-1-I1-63 Ookayama, Meguro-ku. Member AIAA.

Introduction

MANY researchers have investigated the concept of satellite cluster systems in which a group of satellites is coordinated to perform various advanced missions. The benefits of such a system are redundancy and distribution. Each satellite in the cluster features smaller size, lighter weight, and lower cost.[1–3] A typical mission would be, for example, formation flying for interferometer observations in the as part of the of TechSat21[4] and Darwin[5] projects. However, coordinated work in orbit requires significant thruster fuel, and this in turn causes a reduction in satellite lifetime. Beard and Hadaegh proposed a finite thrust control method for a formation rotating at a constant rate in free space.[6] This keeps the relative distances between the spacecraft within specified constraints. This method has the drawback that the reduction of thruster fuel causes decline in the position control accuracy.

As an alternative, many researchers have proposed satellite constellations connected by tethers. Keshmiri et al. formulated the general three-dimensional motion of tethered N-body systems.[7] Tragesser investigated the stability of the spin motion of a tethered ring formation based on the conical Likins–Pringle relative

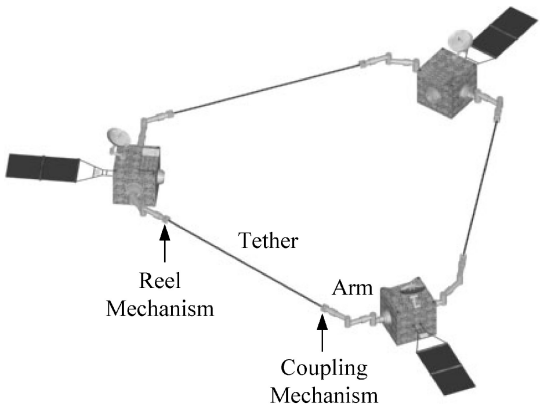

Fig. 1 Tethered satellite cluster system.

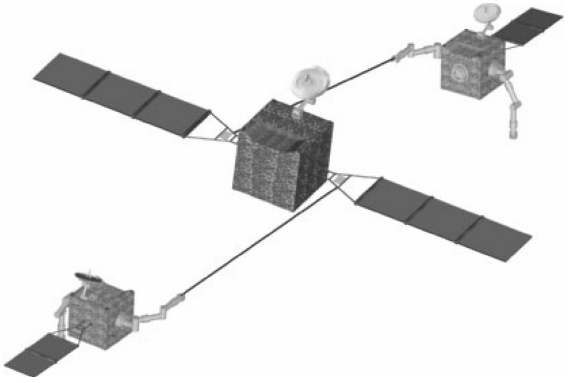

Fig. 2 Tethered multisatellites for in-orbit servicing.

equilibrium.[8] DeCou investigated the dynamics for a triangular formation of satellites.[9] Maccone considered a tethered system to get magnified radio pictures of the galactic center.[10] Yasumitsu and Natori showed the dynamical behavior of a tethered system microsatellite constellation.[11] However, in these studies each satellite is defined as a point mass, and the torque caused by the tether offset is not discussed.

This paper proposes a new tethered satellite cluster system as sketched in Fig. 1. The system consists of tether-connected robotic satellites, which maintain and change formation using active control of the tension and length of each tether. Each satellite has arms and can change the tether offsets by controlling the endpoints of the arms. Thus tether tension can be used for attitude control[12–15] as well as for position control. Such a system can be used in formation flying by using the tether tension not only for saving thruster fuel but also improving the control accuracy of the position and attitude of each satellite. The concept can be applied to tethered multisatellites for in-orbit servicing,[16–19] performing various missions such as autonomic inspection, casting, capture, recovery, moorage, and deorbiting of an uncontrolled satellite, as shown in Fig. 2.

We consider the rotational motion with respect to the c.m. of the system in a formation pattern. Circular motion is treated as the most fundamental case. The equilibrium conditions for maintaining the circular motion using the tether tension are shown, and a control method based on the equilibrium conditions for minimizing thruster fuel is investigated. Next, the equilibrium conditions for a similar transformation of the system are derived, and the control methods for saving fuel are shown. Numerical simulations demonstrate that these control methods are effective in decreasing the relative position/attitude errors of the satellites as well as in reducing the satellite fuel consumption. In addition, we develop a ground experiment system,[20–22] including a reel mechanism[12,23–25] to simulate the tethered satellite cluster system. We outline the system components and verify the dynamics and control methods with two-dimensional experiments.

Tethered Satellite Cluster System

The main features of the proposed tethered satellite cluster system are as follows:

1) The system is reconfigurable by tether connection/disconnection between the satellites.

2) The tether tension and length are controlled by a reel mechanism, and the tether connection/disconnection is effected with a coupling mechanism.

3) The reel or coupling mechanisms are installed on the endpoints of the arms of each satellite.

4) Each satellite maintains formation flying by a coordinated control of position and attitude using the reel, the arm, the thruster, and the reaction wheel.

5) The control system results in reduced fuel consumption and improved relative position/attitude accuracy through control of the tether tension.

We consider the following two fundamental motions: translational motion, which is moving the satellites to an arbitrary position for the transportation of supplies, such as for a space elevator, or for rendezvous docking, etc.; and rotational motion, which is rotating the system about the c.m. while maintaining or changing the formation. This is useful for interferometry measurement, or for stabilization of a solar sail[26,27] or a space solar power system.[28]

Combining the two motions, the system can perform various advanced services, such as capturing an uncontrolled satellite, mooring to space structures, and operating a tethered camera for satellite inspection.

Modeling and Formulation

Figure 3 shows an analytical model of the system. We consider the motions of the n satellites connected by tethers in an Earth-centered inertial coordinate system $\{\boldsymbol{i}\}$. Each satellite, tether, and arm is modeled as follows where $j, k = 1, 2, \ldots, n$, and $j \neq k$.

For satellite j, the body-fixed coordinate system is $\{\boldsymbol{b}_j\}$; the mass is m_j; the position of the c.m. is $\boldsymbol{q}_j$; the moment of inertia about a set of axes passing through its c.m. is $\boldsymbol{I}_j$; and the angular velocity is $\boldsymbol{\omega}_j$.

For tether jk (connects satellites j and k), the tension is $T_{jk}(=T_{kj}) \geq 0$; and the mass, twist moment, bending moment, and tensile strain are ignored.

For arm jk, a three-degree-of-freedom (DOF) arm mounted on satellite j, and controlling the position of the arm end $\boldsymbol{a}_{jk}(\neq \boldsymbol{a}_{kj})$ and the orientation of the reel or the coupling mechanism connected to tether jk.

In this paper, each satellite is in the neighborhood of the c.m. of the system. By the Newton–Euler equations, the motion of each satellite can be formulated as follows:

$$m_j \ddot{\boldsymbol{q}}_j = \frac{\mu m_j}{|\boldsymbol{q}_j|^3}\boldsymbol{q}_j + \boldsymbol{F}_j + \sum_k \boldsymbol{F}_{jk} \tag{1}$$

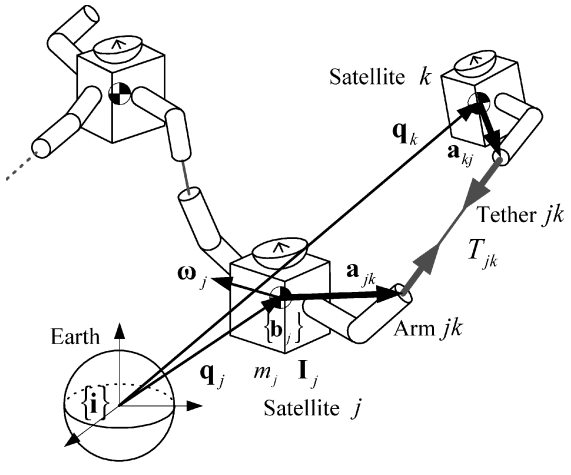

Fig. 3 Analytical model.

$$\boldsymbol{I}_j \cdot \dot{\boldsymbol{\omega}}_j + \boldsymbol{\omega}_j \times \boldsymbol{I}_j \cdot \boldsymbol{\omega}_j = \frac{3\mu}{|\boldsymbol{q}_j|^3}\boldsymbol{q}_j \times \boldsymbol{I}_j \cdot \boldsymbol{q}_j + \boldsymbol{\tau}_j + \sum_k \boldsymbol{\tau}_{jk} \quad (2)$$

The first-order term of the gravity-gradient torque is considered. $\boldsymbol{F}_j$ and $\boldsymbol{\tau}_j$ are the thrust and the torque vectors acting on satellite j as a result of the thruster and the reaction wheel. $\boldsymbol{F}_{jk}$ and $\boldsymbol{\tau}_{jk}$ are the tension and the torque vectors caused by tether jk and are expressed as follows:

$$\boldsymbol{F}_{jk} = T_{jk}\frac{(\boldsymbol{q}_k + \boldsymbol{a}_{kj}) - (\boldsymbol{q}_j + \boldsymbol{a}_{jk})}{|(\boldsymbol{q}_k + \boldsymbol{a}_{kj}) - (\boldsymbol{q}_j + \boldsymbol{a}_{jk})|} \quad (3)$$

$$\boldsymbol{\tau}_{jk} = \boldsymbol{a}_{jk} \times \boldsymbol{F}_{jk} \quad (4)$$

These equations can deal with both an open string of satellites and a closed-ring formation. $\boldsymbol{F}_j$ and $\boldsymbol{\tau}_j$ are external force/torque, and they consume the thruster fuel. On the other hand, $\boldsymbol{F}_{jk}$ and $\boldsymbol{\tau}_{jk}$ are internal force/torque. They are useful for the motion in which the angular momentum is not changed, for example maintaining the rotational motion.

Rotational Motion

We now consider the rotational motion, where n satellites rotate about the c.m. of the system with a desired formation on the same plane. We then establish control methods using the tension of the tether.

Rotational Coordinate System

Figure 4 shows the rotational model in case of $n = 3$. The definition of the rotational coordinate system $\{\boldsymbol{r}\}$ is as follows. The origin of $\{\boldsymbol{r}\}$ is the c.m. of the system,

$$\boldsymbol{q}_{\text{c.m.}} = \frac{\sum_{j=1}^{n} m_j \boldsymbol{q}_j}{\sum_{j=1}^{n} m_j} \quad (5)$$

where $\boldsymbol{r}_x\boldsymbol{r}_y$ represents the desired rotational plane and $\boldsymbol{r}_z$ is the rotational axis. Here $\boldsymbol{r}_x$ shows the direction of H_1: H_j is the foot of perpendicular from the mass center of satellite j to the rotational plane. The relationship between $\{\boldsymbol{r}\}$ and $\{\boldsymbol{i}\}$ is defined by the following 3-2-1 Euler angles:

$$\{\boldsymbol{r}\} = C^3(\varphi_r)\{\boldsymbol{s}\} = C^3(\varphi_r)C^2\left(\theta_r^d\right)C^1\left(\psi_r^d\right)\{\boldsymbol{i}\} \quad (6)$$

where $\{\boldsymbol{s}\}$ is the intermediate coordinate system fixed on the desired rotational plane and the superscript d shows a desired (set) value. Here $\boldsymbol{s}_z$ is the rotational axis ($\boldsymbol{s}_z = \boldsymbol{r}_z$), and the angular velocity of $\{\boldsymbol{r}\}$ with respect to $\{\boldsymbol{s}\}$ is $\dot{\varphi}_r\boldsymbol{r}_z$. The attitude relationship between $\{\boldsymbol{r}\}$, $\{\boldsymbol{s}\}$, and $\{\boldsymbol{i}\}$ is shown in Fig. 4. The angular momentum vector $\boldsymbol{P}$ of this system about c.m. is represented as follows:

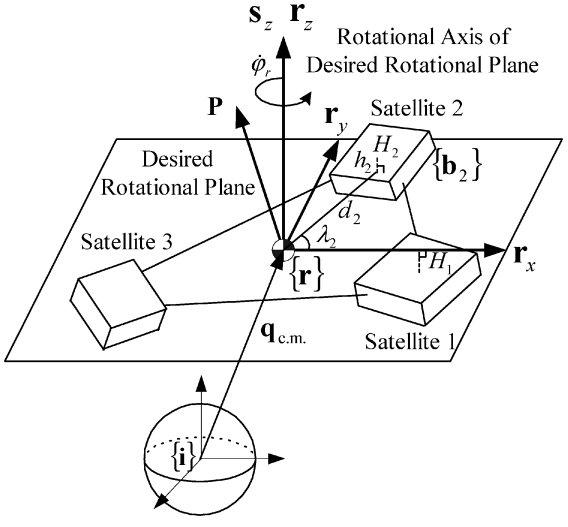

Fig. 4 Rotational coordinate system.

$$\boldsymbol{P} = \sum_{j=1}^{n}[m_j(\boldsymbol{q}_j - \boldsymbol{q}_{\text{c.m.}}) \times (\dot{\boldsymbol{q}}_j - \dot{\boldsymbol{q}}_{\text{c.m.}}) + \boldsymbol{I}_j \cdot \boldsymbol{\omega}_j] \quad (7)$$

The position and attitude of each satellite in $\{\boldsymbol{r}\}$ are defined as follows.

Position:

$$\boldsymbol{q}_j - \boldsymbol{q}_{\text{c.m.}} = \{\boldsymbol{r}\}^T \begin{bmatrix} d_j \cos\lambda_j \\ d_j \sin\lambda_j \\ h_j \end{bmatrix} \quad (8)$$

Attitude:

$$\{\boldsymbol{b}_j\} = C^1(\psi_j)C^2(\theta_j)C^3(\varphi_j)\{\boldsymbol{r}\} \quad (9)$$

where d_j is the distance from the origin of $\{\boldsymbol{r}\}$ to H_j; λ_j is the angle between the two directions of H_j and H_1; and h_j is the distance from H_j to the mass center of satellite j. Given the definition of $\{\boldsymbol{r}\}$, the following equations are satisfied:

$$\sum_{j=1}^{n} m_j \begin{bmatrix} d_j \cos\lambda_j \\ d_j \sin\lambda_j \\ h_j \end{bmatrix} = \begin{bmatrix} 0 \\ 0 \\ 0 \end{bmatrix} \quad (10)$$

$$\lambda_1 = 0 \quad (11)$$

When each satellite is perfectly following the desired rotational motion, the directions of $\boldsymbol{P}$ and $\boldsymbol{r}_z$ are the same, and $h_j = 0$ is satisfied. The position and attitude of each satellite can be obtained by global positioning system and an attitude sensor. Each satellite can use thrusters and reaction wheels for control of the relative position and attitude in formation flying. However, thrusters consume considerable fuel to perform a desired rotational motion. Therefore this paper proposes that the tethered satellite cluster system use the tether tension and torque in order to save thruster fuel and to improve the accuracy of the position and attitude control. This analysis assumes that the spin rate of the formation is much larger than the orbital rate, and so the spin axis of the formation remains in the same inertial direction.

Equilibrium Conditions for Circular Motion

When the system formation in $\{\boldsymbol{r}\}$ is constant, each satellite of the system makes a circle in $\{\boldsymbol{s}\}$. It is defined as a circular motion. If the sum of the tether tensions acting on each satellite is equal to the centrifugal force of the circular motion, the motion is maintained without thruster force:

$$\sum_k \boldsymbol{F}_{jk} = -m_j\dot{\varphi}_r^2(\boldsymbol{q}_j - \boldsymbol{q}_{\text{c.m.}}) \quad (12)$$

and if the torque from the tethers acting on each satellite is equal to zero, the attitude of each satellite in $\{\boldsymbol{r}\}$ is maintained without reaction-wheel torque:

$$\sum_k \boldsymbol{\tau}_{jk} = 0 \quad (13)$$

where $\boldsymbol{\tau}_{jk} = 0$ is satisfied when the arm jk end position $\boldsymbol{a}_{jk} \propto \{(\boldsymbol{q}_k + \boldsymbol{a}_{kj}) - (\boldsymbol{q}_j + \boldsymbol{a}_{jk})\}$. If these equilibrium equations (12) and (13) are satisfied, the translational and rotational angular momentum $m_j d_j^2\dot{\varphi}_r$ and $I_j\omega_j$ of each satellite are conserved.

The system is divided into four connection types: chain connection, loop connection, star connection, and all connection as shown in Fig. 5. The equilibrium formations and tensions, satisfying Eq. (12), are derived as follows.

Chain connection: All satellites are connected in a line as shown in Fig. 5a.

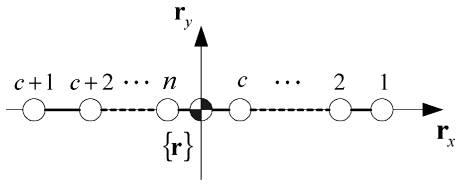

a) Chain connection

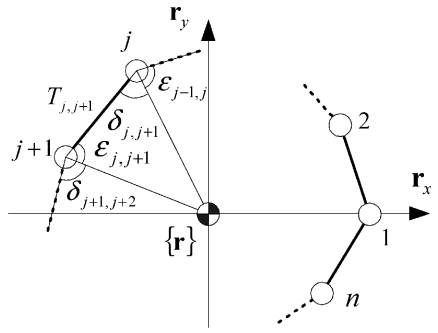

b) Loop connection

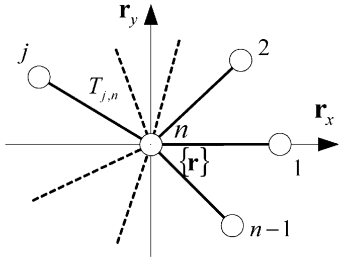

c) Star connection

Fig. 5 Tether-connection types.

Formation:

$$\begin{cases} \lambda_1 = \cdots = \lambda_c = 0, & \lambda_{c+1} = \cdots = \lambda_n = \pi \\ d_1 > \cdots > d_c, & d_{c+1} > \cdots > d_n \end{cases} \tag{14}$$

Tension:

$$\begin{cases} T_{12} = m_1 d_1 \dot{\varphi}_r^2,\ T_{c+1,c+2} = m_{c+1} d_{c+1} \dot{\varphi}_r^2 \\ T_{j,j+1} = T_{j-1,j} + m_j d_j \dot{\varphi}_r^2 \\ T_{cn} = T_{c-1,c} + m_c d_c \dot{\varphi}_r^2 = T_{n-1,n} + m_n d_n \dot{\varphi}_r^2 \end{cases} \tag{15}$$

The bottom equation of Eq. (15) is satisfied because of the definition of $\{\boldsymbol{r}\}$.

Loop connection: Satellites are connected in a ring as shown in Fig. 5b.

Tension:

$$\begin{cases} T_{j,j+1} = \dfrac{m_j d_j \dot{\varphi}_r^2 \sin\delta_{j,j+1}}{\sin(\delta_{j,j+1} + \varepsilon_{j-1,j})} = \dfrac{m_{j+1} d_{j+1} \dot{\varphi}_r^2 \sin\varepsilon_{j,j+1}}{\sin(\delta_{j+1,j+2} + \varepsilon_{j,j+1})} \\ T_{n1} = \dfrac{m_n d_n \dot{\varphi}_r^2 \sin\delta_{n1}}{\sin(\delta_{n1} + \varepsilon_{n-1,n})} = \dfrac{m_1 d_1 \dot{\varphi}_r^2 \sin\varepsilon_{n1}}{\sin(\delta_{12} + \varepsilon_{n1})} \end{cases} \tag{16}$$

Examples of the equilibrium formation are a rhombus, a rectangle, and a regular polygon. A reentrant polygon does not satisfy the conditions because the tension is positive.

Star connection: One central satellite is connected to all other satellites as shown in Fig. 5c.

Formation:

$$d_n = 0 \tag{17}$$

Tension:

$$T_{jn} = m_j d_j \dot{\varphi}_r^2 \tag{18}$$

Equation (17) indicates that the satellite n is at the c.m. of the system.

All connection: All satellites are connected to each other by tethers.

Formation: arbitrary planar formation

Tension:

$$T_{jk} = m_j m_k |\boldsymbol{q}_k - \boldsymbol{q}_j| \frac{\dot{\varphi}_r^2}{\sum_{l=1}^{n} m_l} \tag{19}$$

Although the all-connection type is complicated relatively, it can maintain arbitrary planar formation. Only these types can maintain defined formations by tether tension.

Coordinated Control Method for Circular Motion

Satellite cluster systems can perform a desired circular motion by using the following thruster/reaction-wheel control for each satellite based on proportional and derivative (PD) control.

Thruster/reaction-wheel control.

Thruster:

$$\boldsymbol{F}_j = -m_j \left[C_1 \left(\dot{\boldsymbol{q}}_j - \dot{\boldsymbol{q}}_j^d \right) + K_1 \left(\boldsymbol{q}_j - \boldsymbol{q}_j^d \right) \right] \tag{20}$$

Reaction wheel:

$$\boldsymbol{\tau}_j = -\boldsymbol{I}_j \cdot \left[C_2 \left(\boldsymbol{\omega}_j - \dot{\varphi}_r^d \boldsymbol{r}_z \right) + K_2 \{\boldsymbol{b}_j\}^T \begin{bmatrix} \psi_j - \psi_j^d \\ \theta_j - \theta_j^d \\ \varphi_j - \varphi_j^d \end{bmatrix} \right] \tag{21}$$

Thrusters and reaction wheels are used for feedback control of position and attitude, respectively. If a satellite does not have any reaction wheels, thrusters can be substituted.

Using thrusters to maintain a circular motion would generally require too much fuel. This paper therefore proposes using the following reel/arm control as well as thruster/reaction-wheel control in order to decrease the fuel consumption.

Reel/arm control.

Reel:

$$T_{jk} = T_{jk}^d \tag{22}$$

Arm:

$$\boldsymbol{a}_{jk}^d = l_{jk} \frac{\boldsymbol{q}_k^d - \boldsymbol{q}_j^d}{\left| \boldsymbol{q}_k^d - \boldsymbol{q}_j^d \right|} \tag{23}$$

T_{jk}^d is the equilibrium tension for the desired circular motion in Eqs. (15), (16), (18), and (19), and l_{jk} is the distance between the c.m. of the satellite j and the reel or coupling mechanism connected to tether jk. This is the tether tension/torque feedforward control. When each satellite perfectly follows the desired circular motion, it can maintain the motion without thrust by the reel/arm control. Thus each satellite can save thruster fuel. The various errors and distortions can be tolerated by the feedback control of thruster/reaction wheel (refer to the Appendix).

Equilibrium Conditions for Similar Transformations

Next, we consider the case of a formation changing size but maintaining shape, as shown in Fig. 6. Such a rotational motion is defined as a similar transformation. In this motion, the amount of $\dot{d}_j/d_j$ of each satellite is equal to each other. And λ_j is not changed, and $h_j = 0$ should be satisfied regardless of connection type. If the sum of the tether tensions acting on each satellite is equal to the centrifugal force of the rotational motion, the similar transformation is achieved without thruster force.

$$\sum_k \boldsymbol{F}_{jk} = -m_j \left(\dot{\varphi}_r^2 - \frac{\ddot{d}_j}{d_j} \right) (\boldsymbol{q}_j - \boldsymbol{q}_{\text{c.m.}}) \tag{24}$$

The amount of $\dot{\varphi}_r$ is decided by the conservation of angular momentum. The $\ddot{d}_j/d_j$ term shows the changing ratio of the similar

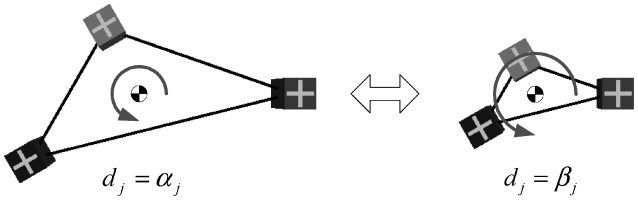

Fig. 6 Similar transformation sequence in the $r_x r_y$ plane.

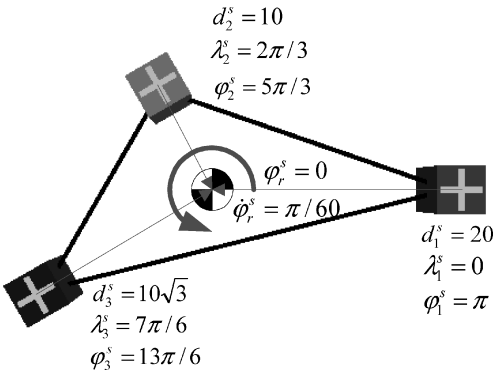

Fig. 7 Simulation conditions.

transformation. In the case of $\ddot{d}_j/d_j = 0$, Eq. (24) becomes equal to Eq. (12). Replacing the $\dot{\varphi}_r^2$ terms with $(\dot{\varphi}_r^2 - \ddot{d}_j/d_j)$ in Eqs. (15), (16), (18), and (19), we arrive at the equilibrium tension T_{jk}^d for the similar transformations. The equilibrium formations for the similar transformations are the same as those for circular motions. Because $T_{jk} \geq 0$, the relationship $\ddot{d}_j/d_j \leq \dot{\varphi}_r^2$ needs to be satisfied.

Control Method for Similar Transformations

The system can take advantage of the equilibrium tension for similar transformations in the control scheme. The coordinated control method for circular motions is also efficient for decreasing fuel usage for similar transformations. The thruster/reaction-wheel control, Eqs. (20) and (21), transfers the system to a desired motion, and the reel/arm control, Eqs. (22) and (23), maintains it.

Numerical Simulations

Consider the rotational motion of three satellites ($n = 3$), all connected to each other, as shown in Fig. 7. The following numerical simulations verify the control methods just proposed.

Simulation Conditions

The following parameters describe the system in meter-kilogram-second (MKS) units.

Satellite shape:

$$m_j = 50, \qquad {}^b I_j = \mathrm{diag}\{2, 2, 2\}, \qquad l_{jk} = 1 \tag{25}$$

Orbital motion:

$$|{}^i q_{\mathrm{c.m.}}| = 570{,}000 \qquad \text{(circular orbit of which period is 5764 s)} \tag{26}$$

Rotational axis and rotational plane:

$$\psi_r^d = \pi/6, \qquad \theta_r^d = \pi/6 \tag{27}$$

Initial conditions:

$$\varphi_r^s = 0, \qquad \dot{\varphi}_r^s = \pi/60 \tag{28}$$

$$d_1^s = 20, \qquad d_2^s = 10, \qquad d_3^s = 10\sqrt{3} \tag{29}$$

$$\lambda_2^s = 2\pi/3, \qquad \lambda_3^s = 7\pi/6, \qquad h_j^s = 0 \tag{30}$$

Table 1 Average of position/attitude errors: circular motion simulation

Tension	$\lvert\Delta q_2\rvert$, mm	$\sqrt{\lvert\Delta\psi_2\rvert^2 + \lvert\Delta\theta_2\rvert^2 + \lvert\Delta\varphi_2\rvert^2}$, deg
$T_{jk} = T_{jk}^d$	0.000	0.000
$T_{jk} = 0$	0.273	0.000
$T_{jk} = 1.5T_{jk}^d$	0.137	0.000

$$\psi_j^s = 0, \qquad \theta_j^s = 0, \qquad \varphi_j^s = \lambda_j^s + \pi \tag{31}$$

$$\dot{\boldsymbol{q}}_j^s = \{\boldsymbol{r}\}^T \begin{bmatrix} -\dot{\varphi}_r^s d_j^s \sin\lambda_j^s & \dot{\varphi}_r^s d_j^s \cos\lambda_j^s & 0 \end{bmatrix}^T \tag{32}$$

$$\boldsymbol{\omega}_j^s = \{\boldsymbol{b}\}^T \begin{bmatrix} 0 & 0 & \dot{\varphi}_r^s \end{bmatrix}^T \tag{33}$$

where the superscript s indicates the initial value. Equation (28) shows the spin angle and angular velocity of the system. Equations (29) and (30) show the triangle formation. Equation (31) shows the attitude of each satellite. These initial conditions are sketched in Fig. 7. Equations (32) and (33) show the velocity and angular velocity vectors of each satellite, respectively.

Circular Motion Simulation

When the initial formation is maintained, each satellite of the system makes a circle. Because $\dot{\varphi}_r^s = \pi/60$, the cycle of the circular motion is 120 s, which is a typical condition for interferometer observations. This motion is set as the desired one. Each satellite can perform the desired motion by the prescribed thruster/reaction-wheel control in Eqs. (20) and (21), adding equilibrium tension T_{jk}^d calculated by Eq. (19).

Figure 8a shows the trajectory of each satellite in the $s_x s_y$ plane. The solid, dashed, and dotted lines represent satellites 1, 2, and 3, respectively, and the system maintains the desired circular motion. The radius of the circular motion of each satellite is d_j^s. Figures 8b and 8c show the accumulated thruster impulse and the accumulated reaction-wheel angular impulse acting on satellite 2. The solid, dashed, and dotted lines represent the three cases of $T_{jk} = T_{jk}^d$ or 0 or $1.5T_{jk}^d$. Table 1 shows the average of the relative position/attitude errors of satellite 2 for each case. The accumulated thruster impulse is proportional to the fuel consumption. In the case of $T_{jk} = T_{jk}^d$, the sum of the tether tensions acting on the satellite is equal to the centrifugal force of the desired circular motion. Thus the thruster force is needed only to correct errors caused by the orbital motion, and the accumulated impulse is small. On the other hand, in the case of $T_{jk} = 0$ or $1.5T_{jk}^d$, the thruster force for maintaining the circular motion is equal to the centrifugal force $m_2 d_2^d \dot{\varphi}_r^{d^2}$ or $-0.5 m_2 d_2^d \dot{\varphi}_r^{d^2}$, respectively. The same is true of the other satellites. Therefore, in the case of $T_{jk} = \alpha T_{jk}^d$, where α is a constant, the accumulated thruster impulse acting on satellite j is represented as follows:

$$\int |F_j| \, \mathrm{d}t \approx |1 - \alpha| m_j d_j^d \dot{\varphi}_r^{d^2} t \tag{34}$$

The accumulated reaction-wheel angular impulse is also related to the thruster fuel consumption because the thruster is substituted for reaction-wheel attitude control. Figure 8c indicates that it is nearly equal to zero in all three cases. The reason is that no torque is required for maintaining the circular motion and that the reaction wheel is used only to correct attitude errors.

In Table 1, the average of the position error is the smallest for the case of $T_{jk} = T_{jk}^d$, and it becomes larger in the cases of $T_{jk} = 1.5T_{jk}^d$ and 0 in that order. The average of the attitude error is equal to zero in the three cases. Similar results are obtained for accumulated thruster impulse and reaction-wheel angular impulse. Therefore the proposed feedforward tension is useful in improving the position control accuracy as well as in reducing the fuel consumption of the thruster.

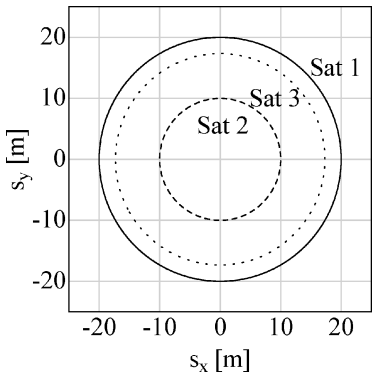

a) Trajectory in the $s_x s_y$ plane

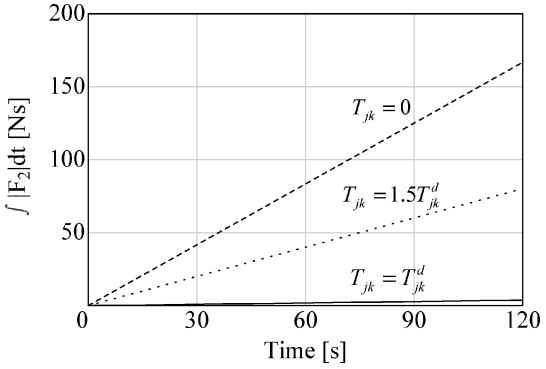

b) Accumulated thruster impulse

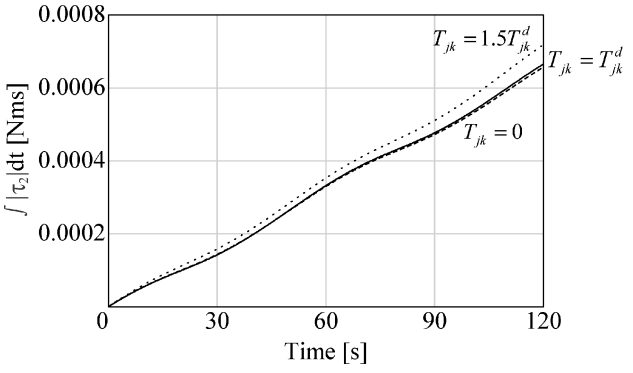

c) Accumulated reaction-wheel angular impulse

Fig. 8 Circular motion simulation.

Similar Transformation Simulation

The following ellipse motion is considered as a desired similar transformation:

$$d_j^d = \frac{\alpha_j \beta_j}{\sqrt{\alpha_j^2 \cos^2 \varphi_r^d + \beta_j^2 \sin^2 \varphi_r^d}} \tag{35}$$

where α_j and β_j are the lengths of the major and minor axes of the ellipse in the $\boldsymbol{s}_x \boldsymbol{s}_y$ plane, respectively. They are set as follows:

$$\alpha_j = d_j^s, \qquad \beta_j = 0.5 d_j^s \tag{36}$$

The equilibrium tension T_{jk}^d and the desired angular velocity $\dot{\varphi}_r^d$ are calculated by the following equations:

$$T_{jk}^d = m_j m_k \left| \boldsymbol{q}_k^d - \boldsymbol{q}_j^d \right| \frac{\left(\dot{\varphi}_r^{d^2} - \ddot{d}_j^d \big/ d_j^d \right)}{\sum_{l=1}^n m_l} \tag{37}$$

$$m_j d_j^{d^2} \dot{\varphi}_r^d = m_j d_j^{s^2} \dot{\varphi}_r^s \tag{38}$$

Because $\dot{\varphi}_r^s = \pi/60$, the cycle of the elliptical motion is 60 s.

Table 2 Average of position/attitude errors: similar transformation simulation

Tension	$\lvert\Delta q_2\rvert$, mm	$\sqrt{\lvert\Delta\psi_2\rvert^2 + \lvert\Delta\theta_2\rvert^2 + \lvert\Delta\varphi_2\rvert^2}$, deg
$T_{jk} = T_{jk}^d$	0.000	0.049
$T_{jk} = 0$	0.843	0.066
$T_{jk} = 1.5T_{jk}^d$	0.420	0.043

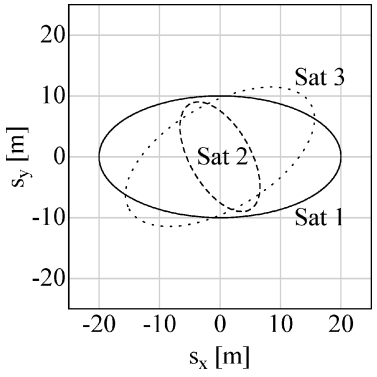

a) Trajectory in the $s_x s_y$ plane

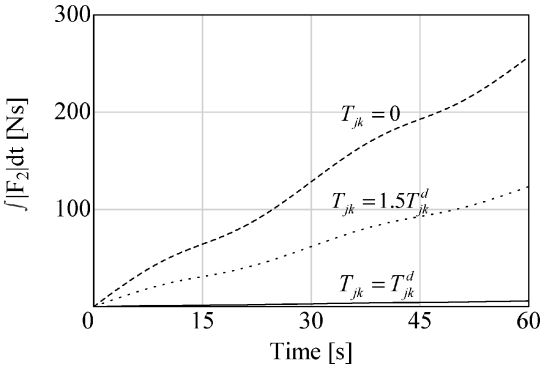

b) Accumulated thruster impulse

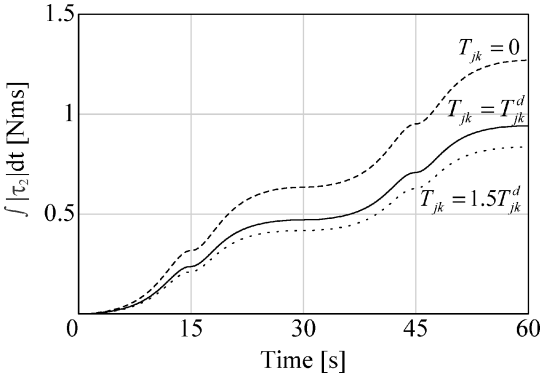

c) Accumulated reaction-wheel angular impulse

Fig. 9 Similar transformation simulation.

Figure 6 shows the transformation sequence of the motion in the $\boldsymbol{r}_x \boldsymbol{r}_y$ plane. Figure 9a shows the trajectory of each satellite in the $\boldsymbol{s}_x \boldsymbol{s}_y$ plane. The solid, dashed, and dotted lines represent the data for satellites 1, 2, and 3, respectively. Figure 9a indicates that the formation of the system changes in size similarly in the $\boldsymbol{r}_x \boldsymbol{r}_y$ plane and that each satellite performs the desired elliptical motion in the $\boldsymbol{s}_x \boldsymbol{s}_y$ plane. Figures 9b and 9c show the accumulated thruster impulse and the accumulated reaction-wheel angular impulse working on satellite 2. The solid, dashed, and dotted lines represent the three cases of $T_{jk} = T_{jk}^d$, 0, and $1.5T_{jk}^d$. Table 2 shows the average of the relative position/attitude errors of satellite 2 for each case. In Fig. 9b, the sum of the tether tensions in the case of $T_{jk} = T_{jk}^d$ is

equal to the centrifugal force of the desired elliptical motion, and the accumulated thruster impulse is small. The larger the difference between T_{jk} and T^d_{jk}, the larger the accumulated thruster impulse becomes. In general, the accumulation of the thruster impulse for the case of $T_{jk} = \alpha T^d_{jk}$, where α is a constant, is shown as follows:

$$\int |F_j| \, \mathrm{d}t \approx |1 - \alpha| \int m_j d^d_j \left(\dot{\varphi}^{d^2}_r - \frac{\ddot{d}^d_j}{d^d_j} \right) \mathrm{d}t \tag{39}$$

The graph inclination in Fig. 9b changes cyclically, which corresponds to the centrifugal force of the elliptical motion.

The larger the tension becomes, the smaller the accumulated reaction wheel angular impulse becomes in Fig. 9c. In a similar transformation, the desired angular velocity $\dot{\varphi}^d_r$ changes cyclically. Therefore a torque $I^d_j \ddot{\varphi}^d_r$ is necessary for the attitude control of each satellite. In the case of $T_{jk} = 0$, the accumulated reaction-wheel angular impulse is nearly equal to

$$\int I^d_j \ddot{\varphi}^d_r \, \mathrm{d}t$$

On the other hand, in the case of $T_{jk} \neq 0$, each tether provides the satellites with torque to correct all attitude errors. Because the torque is proportional to the tension, the accumulated reaction-wheel angular momentum becomes smaller with an increase of the tension.

Figures 9b and 9c and Table 2 indicate that the relative position and attitude errors become smaller with a decrease of the thruster impulse and the reaction-wheel angular impulse. Substituting the tether tension/torque for the thruster and the reaction wheel, we see that each satellite can save thruster fuel and improve the position and attitude control accuracy. The accumulated thruster impulse becomes the smallest in the case of $T_{jk} = T^d_{jk}$. However, the accumulated reaction-wheel angular impulse becomes the smallest in the case of $T_{jk} = 1.5T^d_{jk}$ (maximum tension case).

Sketch of a Two-Dimensional Ground Experiment System

Figure 10 shows the two-dimensional ground experiment system[20,21] described in this paper. The system consists of satellite simulators and a ground station as shown in Fig. 10b. Next is a description of the components.

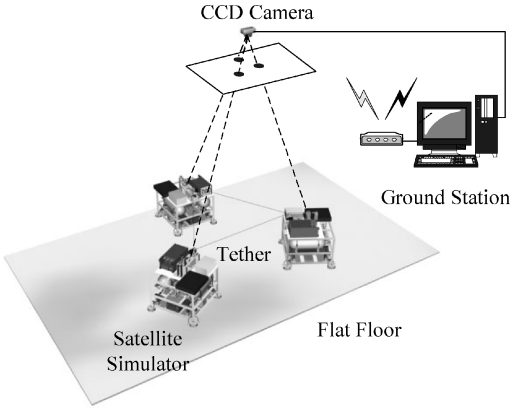

a) System configuration

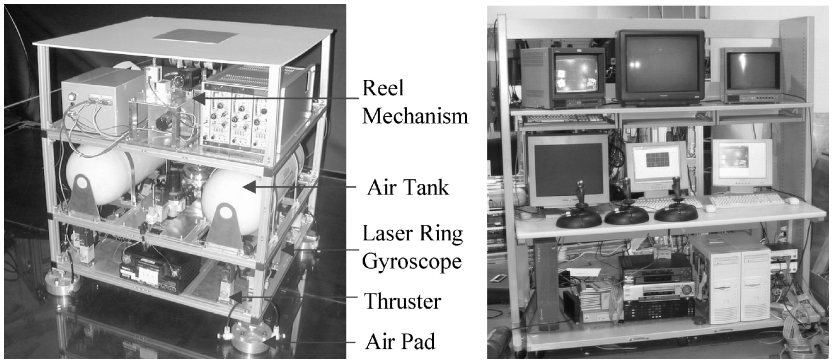

b) Satellite simulator and ground station

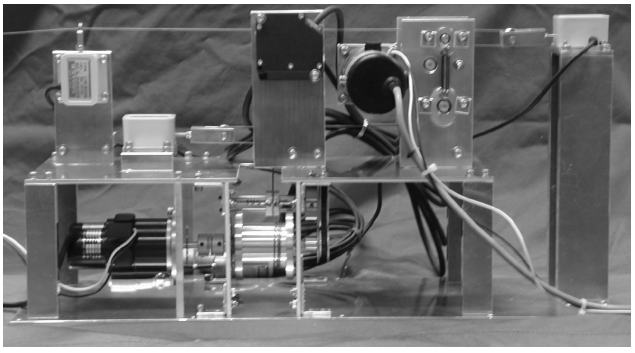

c) Reel mechanism

Fig. 10 Two-dimensional ground experiment system.

Satellite Simulator

Each satellite is a solid rectangular parallelepiped ($0.6 \times 0.6 \times 0.7$ m, $m_j = 58$ kg, $I_j = 3.73$ kgm^2), floating on a flat floor (3×5 m) with four air pads. The driving force/torque is generated with eight thrusters. In these experiments, the satellites are not equipped with reaction wheels. Thus the thrusters control both the position and attitude of each satellite. The force and torque of one thruster is 2.22 N and 0.444 Nm. (Specific impulse is 24.1 s.) Fuel for the thrusters and air pads is supplied by two air tanks. A laser ring gyroscope provides the attitude data of the satellite and the onboard PC communicates with the ground station by wireless LAN (TCP/IP protocol). In the experiments, the reel mechanisms[12,23] as shown in Fig. 10c are mounted on the satellite. The size is $140 \times 400 \times 200$ mm, and the weight is 3.95 kg. The main function of the reel mechanism is to deploy and retract the tether. The reel mechanism also serves the following functions: 1) to avoid a jam in the case the tension is nearly zero, 2) to measure tension and direction of the tether, 3) to wind the tether on the reel uniformly, and 4) to measure the deployed length of the tether.

Ground Station

A charge-coupled-device camera captures a picture of the whole motion area, and a PC calculates the position of the satellites by pattern matching. The PC also controls the position/attitude of each satellite through the wireless network.

Ground Experiments

We performed two experiments with the tethered satellite cluster system; a circular motion experiment using three satellite simulators ($n = 3$) and a similar transformation experiment using two satellites ($n = 2$).

Experimental Conditions

Figure 11 shows the experimental conditions. The system rotates about the c.m. of the system, and the desired formations are a regular triangle for the circular motion and a line segment for the similar transformation. The tether connection point for each satellite is fixed ($l_{jk} = 0.26$ m). The initial conditions are set as $\varphi_r^s = 0$, $\dot{\varphi}_r^s = 2\pi/30$ rad/s, $d_j^s = 0.8$ m, $\lambda_j^s = 2\pi(j-1)/n$, and $\varphi_j^s = \lambda_j^s + \pi$. In this ground experiment system, the motion of each satellite is limited to two dimensions, and $\psi_j^s = 0$, $\theta_j^s = 0$, and $h_j^s = 0$ are satisfied.

Circular Motion Experiment

The desired motion of each satellite is defined as the circular motion that is caused by maintaining initial motions. Each satellite conducts coordinated control of the reel and thruster to achieve the desired motion. The cycle period of the circular motion is 30 s because $\dot{\varphi}_r^s = 2\pi/30$ rad/s. The equilibrium tension T_{jk}^d of each tether is 1.18 N by Eq. (19).

Figure 12a shows the trajectory of satellite 1 in the $s_x s_y$ plane. The trajectories of satellites 2 and 3 are almost the same. The results

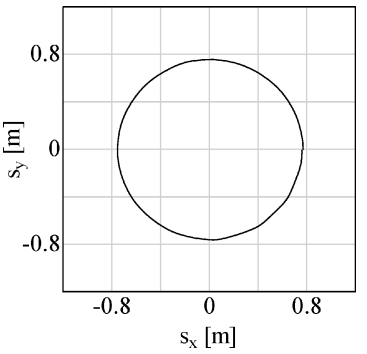

a) Trajectory of satellite 1 in the $s_x s_y$ plane

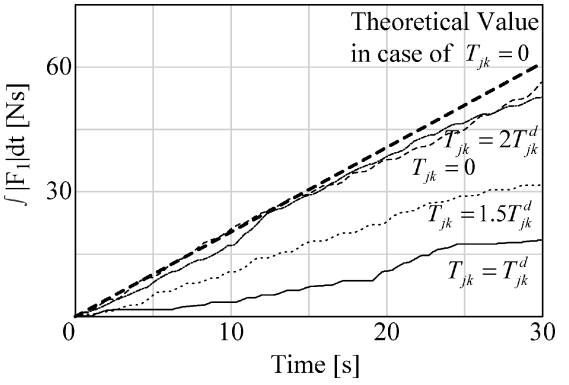

b) Accumulated thruster impulse

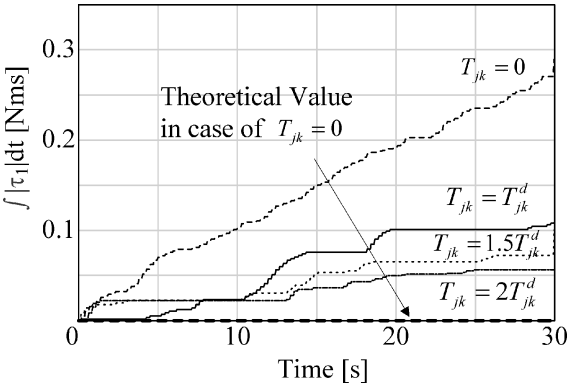

c) Accumulated thruster angular impulse

Fig. 12 Circular motion experiment.

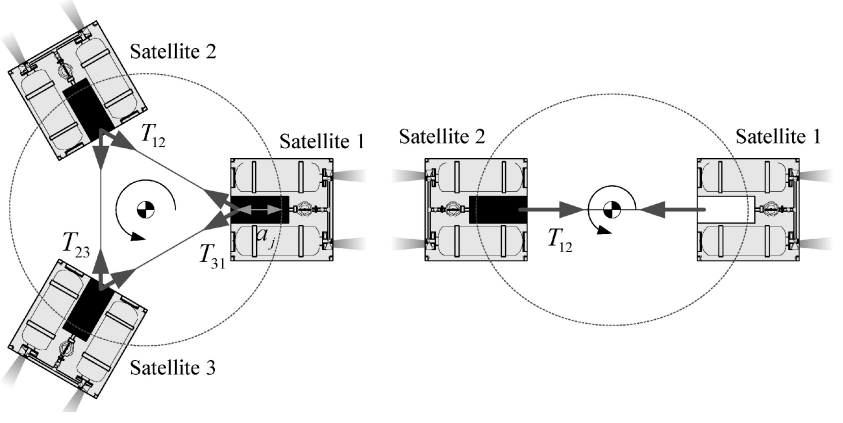

Fig. 11 Experimental conditions (circular and ellipse cases).

Table 3 Average of position/attitude errors: circular motion experiment

Tension	$\|\Delta q_1\|$, mm	$\|\Delta\varphi_1\|$, deg
$T_{jk} = T^d_{jk}$	24.7	4.36
$T_{jk} = 0$	31.3	7.00
$T_{jk} = 1.5T^d_{jk}$	34.1	3.61
$T_{jk} = 2T^d_{jk}$	45.7	4.83

indicate that the system maintains the desired circular motion. Figures 12b and 12c show the accumulated thruster impulse and the accumulated thruster angular impulse acting on the satellite 1. The solid, dashed, dotted, and dot–dashed lines represent, respectively, the four cases of $T_{jk} = T^d_{jk}$ or 0 or $1.5T^d_{jk}$ or $2T^d_{jk}$. The bold broken line represents the following theoretical values in the case of $T_{jk} = 0$ (no tether):

$$\int |F_1|\,\mathrm{d}t = m_1 d_1^d \dot{\varphi}_r^{d^2} t, \qquad \int |\tau_1|\,\mathrm{d}t = \int \left| I_j^d \ddot{\varphi}_r^d \right| \mathrm{d}t = 0 \quad (40)$$

In the case of $T_{jk} = T^d_{jk}$, the accumulated thruster impulse is the smallest, however, not equal to zero, because of the friction and inclination of the flat floor, tension control error, and pattern matching error. The accumulated impulse in the case of $T_{jk} = 0$ is nearly equal to the theoretical value as shown in Eq. (40). It is also nearly equal to the case of $T_{jk} = 2T^d_{jk}$. Note that thrust directions in the cases of $T_{jk} = 0$ and $2T^d_{jk}$ are opposite to each other. The accumulated impulse in the case of $T_{jk} = 1.5T^d_{jk}$ becomes the average value of the impulses in the case of $T_{jk} = T^d_{jk}$ and $2T^d_{jk}$. The fuel mass difference between the two cases $T_{jk} = T^d_{jk}$ and 0 is 0.0726 kg (specific impulse is 24.1 s) per circular cycle. These results indicate that the tether tension saves thruster fuel in the case of $T_{jk} = T^d_{jk}$.

None of the accumulated thruster angular impulses in all cases of T_{jk} is equal to zero because of the friction and inclination of the flat floor and position control error. The larger the tension becomes, the smaller the accumulated angular impulse becomes. This is because the tether torque to correct the attitude error is proportional to the tension.

Table 3 shows the average of the position/attitude errors of satellite 1 for each case. The results for other satellites are nearly equal to those of satellite 1. The average of the position error is the smallest in case of $T_{jk} = T^d_{jk}$. The average of the attitude error is the largest in case of $T_{jk} = 0$ because the tension torque is the smallest (zero) in this case.

Similar Transformation Experiment

As a similar transformation, each satellite performs the elliptical motion defined in Eq. (35). The long and short radii are set as $\alpha_j = d_j^s$, $\beta_j = 0.85 d_j^s$, respectively. The cycle period of the elliptical motion is 25.5 s.

Figure 13a shows the trajectory of satellite 1. Figures 13b and 13c show the accumulated thruster impulse and the accumulated thruster angular impulse acting on satellite 1. The solid, dashed, and dotted lines represent the three cases of $T_{jk} = T^d_{jk}$ or 0 or $1.5T^d_{jk}$. The bold broken line represents the following theoretical values in the case of $T_{jk} = 0$ (no tether):

$$\int |F_1|\,\mathrm{d}t = \int m_1 d_1^d \left(\dot{\varphi}_r^{d^2} - \frac{\ddot{d}_1^d}{d_1^d} \right) \mathrm{d}t$$

$$\int |\tau_1|\,\mathrm{d}t = \int \left| I_1^d \ddot{\varphi}_r^d \right| \mathrm{d}t \quad (41)$$

Table 4 shows the average of the position/attitude errors of satellite 1 for each case.

In the case of $T_{jk} = T^d_{jk}$, the accumulated thruster impulse is the smallest, however, not equal to zero, because of the same errors as mentioned in the preceding circular motion experiment. The accumulated impulse in the case of $T_{jk} = 0$ is nearly equal to the theoretical value.

Table 4 Average of position/attitude errors: similar transformation experiment

Tension	$\|\Delta q_1\|$, mm	$\|\Delta\varphi_1\|$, deg
$T_{jk} = T^d_{jk}$	21.2	3.31
$T_{jk} = 0$	33.0	9.20
$T_{jk} = 1.5T^d_{jk}$	37.3	3.36

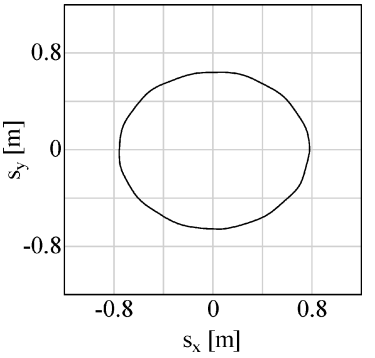

a) Trajectory of satellite 1 in the $s_x s_y$ plane

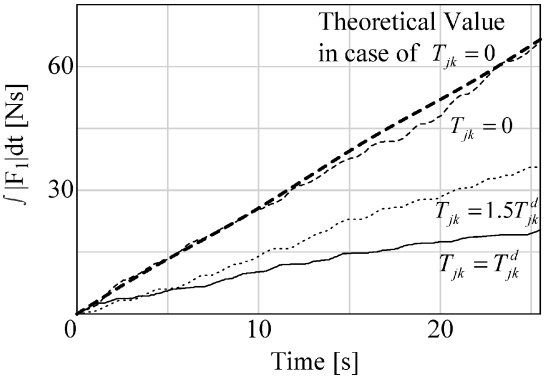

b) Accumulated thruster impulse

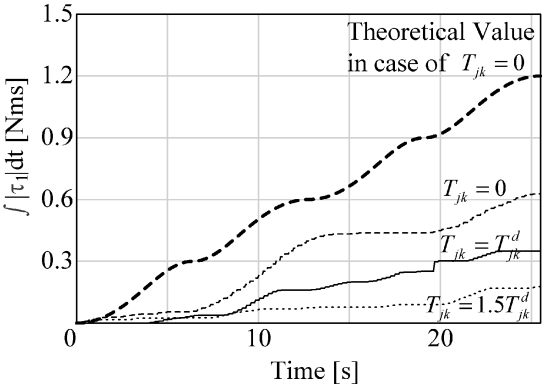

c) Accumulated thruster angular impulse

Fig. 13 Similar transformation experiment.

The accumulated thruster angular impulse is the largest in the case of $T_{jk} = 0$. The larger the tension, the smaller the accumulated angular impulse.

The average of the position error is the smallest in the case of $T_{jk} = T^d_{jk}$, and the average of the attitude error is the largest in the case of $T_{jk} = 0$ in Table 4. These are the same conclusions as with the circular motion experiment.

Conclusions

This paper has discussed the dynamics of tethered satellite clusters in orbit. The control for a same-plane formation rotating with respect to the c.m. of the system was developed and evaluated. The following conclusions were made:

1) The paper presented the equilibrium conditions for maintaining system formation and performing a circular motion by tether tension.

2) The paper presented a coordinated control method for circular motion that minimizes thruster fuel by using the reel, arm, thruster, and reaction wheel.

3) The paper presented the equilibrium conditions for changing the system formation in size similarly.

4) The paper presented a coordinated control method for similar transformations.

5) Numerical simulations and ground experiments were conducted and showed that these control methods can save thruster fuel and improve control accuracy of the position/attitude of each satellite, using the tether tension/torque in addition to the thruster force/reaction-wheel torque.

Appendix: Equation Form of Circular Motion

Newton–Euler Equations (1) and (2) are described by elements of vectors as follows:

$$m_j {}^i\ddot{q}_j = \frac{\mu m_j}{\left|{}^i q_j\right|^3} {}^i q_j + {}^i F_j + \underline{\sum_k \frac{{}^i q_k + {}^i a_{kj} - {}^i q_j - {}^i a_{jk}}{\left|{}^i q_k + {}^i a_{kj} - {}^i q_j - {}^i a_{jk}\right|} T_{jk}} \quad \text{(A1)}$$

$${}^b I_j {}^b\dot{\omega}_j + {}^b\tilde{\omega}_j {}^b I_j {}^b\omega_j = \frac{3\mu}{\left|{}^b q_j\right|^3} {}^b\tilde{q}_j {}^b I_j {}^b q_j + {}^b\tau_j$$

$$+ \underline{\sum_k {}^b\tilde{a}_{jk} \frac{{}^b q_k + {}^b a_{kj} - {}^b q_j - {}^b a_{jk}}{\left|{}^b q_k + {}^b a_{kj} - {}^b q_j - {}^b a_{jk}\right|} T_{jk}} \quad \text{(A2)}$$

The last terms of Eqs. (A1) and (A2) are relating to tension and torque of tether, respectively. They are unique to tethered satellite cluster system. Each satellite can control the motion by modifying parameters T_{jk} and ${}^b a_{jk}$ as well as ${}^i F_j$ and ${}^b\tau_j$. If Eqs. (22) and (23) are satisfied, these terms become $({}^i q_k - {}^i q_j/|{}^i q_k - {}^i q_j|)T_{jk}^d$ and 0, respectively. In case of the circular motion of all-connection type, Eqs. (A1) and (A2) are rewritten as follows, considering Eqs. (5) and (19):

$$m_j {}^i\ddot{q}_j = \frac{\mu m_j}{\left|{}^i q_j\right|^3} {}^i q_j + {}^i F_j + m_j \left|{}^i q_k - {}^i q_{\text{c.m.}}\right| \dot{\varphi}_r^2 \quad \text{(A3)}$$

$${}^b I_j {}^b\omega_j + {}^b\tilde{\omega}_j {}^b I_j {}^b\omega_j = \frac{3\mu}{\left|{}^b q_j\right|^3} {}^b\tilde{q}_j {}^b I_j {}^b q_j + {}^b\tau_j + 0 \quad \text{(A4)}$$

The motion equations of the other connection types are described as the same. Thus the circular motion can be maintained, if ${}^i F_j = -(\mu m_j/|{}^i q_j|^3){}^i q_j$ and ${}^b\tau_j = -(3\mu/|{}^b q_j|^3){}^b\tilde{q}_j {}^b I_j {}^b q_j$ are satisfied by the feedback controls of Eqs. (20) and (21). In this paper, they are small relatively because the orbital rate is supposed to be much larger than the spin rate of the formation.

References

[1]Hansen, E., Colaprete, A., and Rodier, D., "Three Corner Sat Constellation: C&DH, Stereoscopic Imaging, and End-to-End Data System," AIAA/USU, Paper SSC99-IV-1, Aug. 1999.

[2]Horan, S., and Anderson, B., "Three Corner Sat Constellation—New Mexico State University: Communications, LEO Telecommunications Services, Intersatellite Communications, and Ground Stations and Network," AIAA/USU, Paper SSC99-VI-7, Aug. 1999.

[3]Matunaga, S., Mori, O., Kanzawa, T., Tsurumi, S., and Maeda, N., "Concept of Robot Satellite Cluster and Ground Experiment System," *Proceedings of TITech COE/Super Mechano-Systems Workshop*, Tokyo Inst. of Technology, Tokyo, 2000, pp. 103–111.

[4]Schilling, J. H., Spores, R. A., and Spanjers, G. G., "Micropropulsion Options for the TechSat21 Space-Based Radar Flight," *Micropropulsion for Small Spacecraft*, edited by M. M. Micci and A. D. Ketsdever, Vol. 187, Progress in Astronautics and Aeronautics, AIAA, Reston, VA, 2000, pp. 3–23.

[5]Landgraf, M., Jehn, R., Flury, W., Fridlund, M., Karlsson, A., and Léger, A., "IRSI/Darwin: Peering Through the Interplanetary Dust Cloud," *ESA Bulletin*, Vol. 105, Feb. 2001, pp. 60–64.

[6]Beard, R. W., and Hadaegh, F. Y., "Finite Thrust Control for Satellite Formation Flying with State Constraints," *American Control Conference*, American Automatic Control Council, San Diego, CA, 1999, pp. 2975–2979.

[7]Keshmiri, M., Misra, A. K., and Modi, V. J., "General Formulation for N-Body Tethered Satellite System Dynamics," *Journal of Guidance, Control, and Dynamics*, Vol. 19, No. 1, 1996, pp. 74–83.

[8]Tragesser, S. G., "Formation Flying with Tethered Spacecraft," AIAA Paper 2000-4133, Aug. 2000.

[9]DeCou, A. B., "Tether Static Shape for Rotating Multimass, Multitether, Spacecraft for 'Triangle' Michelson Interferometer," *Journal of Guidance, Control, and Dynamics*, Vol. 12, No. 2, 1989, pp. 273–275.

[10]Maccone, C., "Tethered System to Get Magnified Radio Pictures of the Galactic Center from a Distance of 550 AU," *Acta Astronautica*, Vol. 45, No. 2, 1999, pp. 109–114.

[11]Yasumitsu, R., and Natori, M. C., "A Tether System Using Microsatellites Constellation and Its Dynamical Behavior," International Symposium on Space Technology and Science, Paper 2000-k-23, May 2000.

[12]Mori, O., and Matunaga, S., "Research and Development of Tethered Satellite Cluster Systems," International Conf. on Intelligent Robots and Systems, Paper F-AI-5-2, Oct. 2000.

[13]Moccia, A., Vetrella, S., and Grassi, M., "Attitude Dynamics and Control of a Vertical Interferometric Radar Tethered Altimeter," *Journal of Guidance, Control, and Dynamics*, Vol. 16, No. 2, 1993, pp. 264–269.

[14]Pradhan, S., Modi, V. J., and Misra, A. K., "On the Offset Control of Flexible Nonautonomous Tethered Two-Body Systems," *Acta Astronautica*, Vol. 38, No. 10, 1996, pp. 783–801.

[15]Hokamoto, S., "Dynamics of a Space Robot with Tether Tension," *Proceedings of 10th Workshop on Astrodynamics and Flight Mechanics*, Inst. of Space and Astronautical Science, Sagamihara, Japan, 2000, pp. 237–242.

[16]Matunaga, S., Ohkami, Y., and Mori, O., "A Tether-Based Capture of Orbiting Objects," International Astronautical Congress, Paper 97-A.3.08, Oct. 1997.

[17]Matunaga, S., Mori, O., Nakaya, K., and Ohkami, Y., "Tether Control Methods for Damping Angular Momentum of Uncontrolled Satellites," *Proceedings of 8th Workshop on Astrodynamics and Flight Mechanics*, Inst. of Space and Astronautical Science, Sagamihara, Japan, 1998, pp. 310–315.

[18]Kumar, K. D., and Nakajima, A., "Angular Momentum Damping of Debris Through Tether System," International Symposium on Space Technology and Science, Paper 2000-k-20, May 2000.

[19]Nohmi, M., Terumichi, Y., and Sogabe, K., "Modeling of Tethered Space Robot as String-Rigid Bodies," *Proceedings of 10th Workshop on Astrodynamics and Flight Mechanics*, Inst. of Space and Astronautical Science, Sagamihara, Japan, 2000, pp. 243–248.

[20]Hayashi, R., "Capturing Experiments Using Two Dimensional Floating Testbed," International Symposium on Space Technology and Science, Paper 98-n-04, May 1998.

[21]Okada, H., Tsurumi, S., Mori, O., and Matunaga, S., "Development of a Ground Simulation System for RoboSat Clusters," *Proceedings of 11th Workshop on Astrodynamics and Flight Mechanics*, Inst. of Space and Astronautical Science, Sagamihara, Japan, 2001, pp. 377–382.

[22]Adams, J., Robertson, A., Zimmerman, K., and How, J., "Technologies for Spacecraft Formation Flying," *Proceedings of the Institute of Navigation GPS-96 Conference*, Inst. of Navigation, Kansas City, MO, 1996, pp. 1321–1330.

[23]Nakaya, K., Matunaga, S., Mori, O., and Ohkami, Y., "Tether Control Experiments for Damping Angular Momentum of Uncontrolled Satellites," *Proceedings of 9th Workshop on Astrodynamics and Flight Mechanics*, Inst. of Space and Astronautical Science, Sagamihara, Japan, 1999, pp. 37–42.

[24]Nagata, T., "Development of a Reel System for Tethers and its Deployment/Retrieval Test," *Proceedings of 8th Workshop on Astrodynamics and Flight Mechanics*, Inst. of Space and Astronautical Science, Sagamihara, Japan, 1998, pp. 304–309.

[25]Nakamura, Y., Sakamoto, Y., Hirayama, H., and Yasaka, T., "Study of a Tether Deployment System (TDS) of a Micro Tethered Satellite," International Symposium on Space Technology and Science, Paper 2000-d-09, May 2000.

[26]Nakashino, K., and Natori, M. C., "Shape Characteristics of Spin-Stabilized Structures Under Microgravity Environment," AIAA Paper 2001-1344, April 2001.

[27]Matunaga, S., Mori, O., Nakaya, K., Iai, M., Omagari, K., and Yabe, H., "New Spinning Deployment Method of Large Thin Membranes with Tether Control," International Astronautical Congress, Paper 03-A.4.01, Sept. 2003.

[28]Fujii, H. A., Taniue, M., Kojima, H., Mirase, T., Pellegrino, S., and Sasaki, S., "Attitude Stabilization of a Tethered Solar Power Satellite," International Symposium on Space Technology and Science, Paper 2002-d-44, May 2002.

D. Spencer
Associate Editor